Heliyon 9 (2023) e22904

Contents lists available at ScienceDirect

Heliyon

journal homepage: www.cell.com/heliyon

Tracing provenance of eolian sands in the northern Ulan Buh Desert, China: Evidence from the REE geochemical characteristics

Weiyuan Kong [a,b,*], Shangzhe Zhou [a,b], Guipeng Cui [a,b], Pan Gao [a,b], Shuai Li [c], Qi Lu [a,b]

[a] Institute of Ecological Conservation and Restoration, Chinese Academy of Forestry, Beijing, 100091, China
[b] Institute of Desertification Studies, Chinese Academy of Forestry, Beijing, 100091, China
[c] Experimental Center of Desert Forestry, Chinese Academy of Forestry, Dengkou, 015200, Inner Mongolia, China

ARTICLE INFO

Keywords:
Desertification
Sand provenance
Rare earth elements
Sand belts
Ulan Buh Desert

ABSTRACT

Desertification is a primary threat to crop farming, the livestock industry, and the eco-environment in northwestern China. Through field research and satellite imagery, it has been discovered that there are 4–5 sand belts in the shape of handclasps connecting major deserts in the Alxa Plateau region of northern China. These sand belts have been expanding for several decades. However, eolian sand transport between major deserts through these expanding sand belts is still underestimated. Identifying the source areas of eolian sands in deserts provide essential knowledge to prevent desertification. In this study, we collected samples from the northern Ulan Buh Desert (UBD), the Yamalik Desert (YD), and the Langshan Mountains and analyzed their REE contents in the <125 μm fraction. We compared REE geochemical characteristics of fine-grained sands in the UBD with other recently published REE data for potential source areas. Our findings indicate that the primary origins of fine-grained sands in the northern UBD are from the Qilian Mountains (QM) and Badain Jaran Desert (BJD), which are transported through the YD. Contributions from the Gobi-Altay Mountains to the north are relatively minor. The Langshan Mountains and Hawula Mountains are not considered as the primary sources of fine-grained sands in the UBD. In contrast, surface sediments in the southern UBD have a local mixture of the paleo-lacustrine deposits, the Gobi sediments, and minor external inputs from the BJD and QM. Our findings demonstrate that sand belts connecting these deserts play a crucial role in the eolian transport of fine-grained sands. Therefore, both the Chinese government and scientists should pay close attention to them in future efforts to combat desertification.

1. Introduction

The arid climate of northwestern China and neighboring Mongolia has resulted in an extensive distribution of deserts in inland Asia, serving as the primary source of Asian dust to the North Pacific and having a significant impact on biogeochemical cycles and climate [1]. Desertification is one of the most serious threats to human society and ecosystems in these arid and semi-arid areas. Desertification in China is primarily the result of climate change, particularly strong wind regimes, decreased precipitation, and the resulting geomorphological processes [2]. Aside from climate change, human activities such as farming and overgrazing have reduced

* Corresponding author. Institute of Ecological Conservation and Restoration, Chinese Academy of Forestry, Beijing, 100091, China.
E-mail address: wykong@caf.ac.cn (W. Kong).

https://doi.org/10.1016/j.heliyon.2023.e22904
Received 15 April 2023; Received in revised form 15 November 2023; Accepted 22 November 2023
Available online 27 November 2023

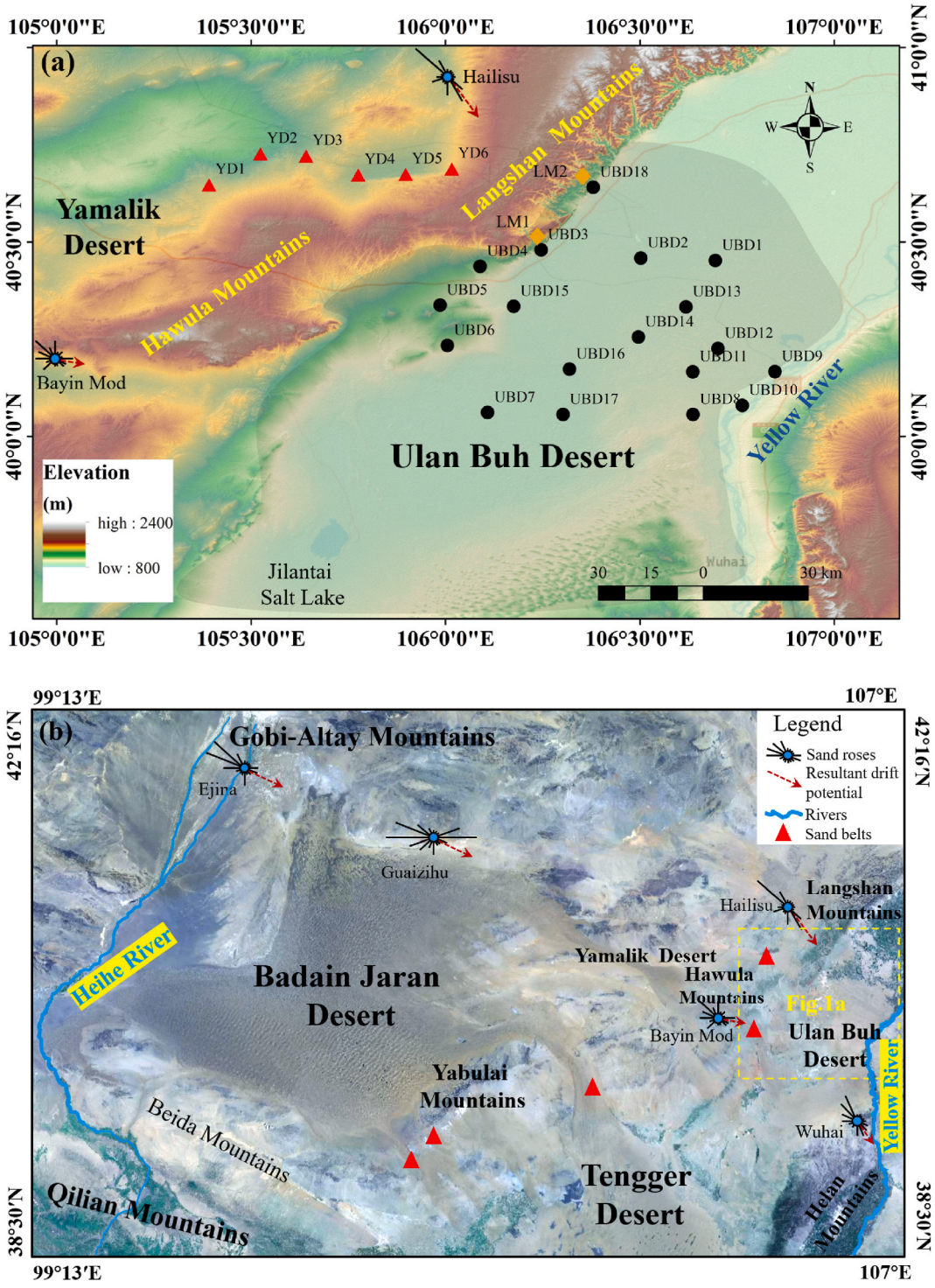

Fig. 1. (a) Sampling site distribution of surface sediments in the UBD (black circles) and the YD (red triangles), as well as bedrocks of the LM (orange diamonds). (b) Map indicating the potential source areas of eolian sands to the study area. The sand rose diagrams for each meteorological station were obtained from Refs. [7,8], with black lines indicating the wind directions capable of transporting sand and red arrows showing the trends of sand transport.

vegetation cover and increased sand transport, resulting in accelerated desertification. To prevent desertification, the Chinese government has implemented a series of countermeasures such as "grain-for-green" and grazing exclusion practices [3]. Researches in tracing sand provenance are critical for understanding mechanisms of desert formation and eolian sand transport, preventing desertification, and forecasting the effects of future climate change scenarios in arid lands [4].

In the Alxa Plateau (AP) of northwest China, there are three major deserts, i.e., the Badain Jaran Desert (BJD), the Tengger Desert (TD), and the Ulan Buh Desert (UBD). In addition to these vast sand seas, the Yamalik Desert (YD), a zonal distributed narrow desert in the AP, lies between the BJD and the UBD. Eolian and fluvial processes transport sediments from the Qilian Mountains (QM), the Gobi-Altay Mountains (GAM), and the peripheral Gobi to the AP deserts. Several interconnecting sand belts have formed between these deserts, dubbed the "Burst and Handclasp" by the local government [5], and eolian sands from the BJD can transport to the TD, YD, and UBD via these passages, as observed in satellite images (Fig. 1b). The shape effects of these sand belts provide favorable conditions for eolian sand transport from the BJD to the TD and UBD, and facilitate the sand recharge to the UBD [6]. Among these sand belts, two of them split at 40.5°N, invading from the eastern YD to the northern and southern UBD, respectively. The northern branch across the interior mountains between the YD and the northern UBD has been rapidly expanding in recent years, enhancing the eolian sand transport of the BJD-YD-UBD conveyer [5] and posing severe challenges to crop farming, livestock industry, and local eco-environment.

The UBD is surrounded by the Langshan Mountains (LM) to the north, the Helan Mountains (HLM) to the south, the Hawula Mountains (HM) to the west, and the Yellow River (YR) to the east. The UBD's flat and wide landform makes it a primary passage for eolian sand and dust transport eastward to North China. However, the formation and evolution of UBD have been debated over the past several decades. Previous research discovered numerous paleolakes in the UBD during the late Quaternary, most notably the Jilantai-Hetao Mega-paleolake. The pioneered work by Hou and Yu [9] suggested that the UBD was formed by de-farming during the Han Dynasty, ~2000 years ago, confirmed by OSL dating results [10]. The radiocarbon dating of paleolake deposits revealed that the UBD resulted from the early Holocene's dry climate [11–13]. According to OSL dating of the deep-drilled sediments, a Mega-paleolake once covered most areas of the UBD until ~90 ka; as the paleolake dried up, modern desert landforms developed simultaneously in the southern and northern UBD [14–16].

The eolian sand provenances of the modern UBD are quite complicated. When paleolake levels fell, many lacustrine deposits were released into the UBD, becoming an important source of eolian sand [7,8,17]. Besides the paleo-lacustrine deposits, other sources

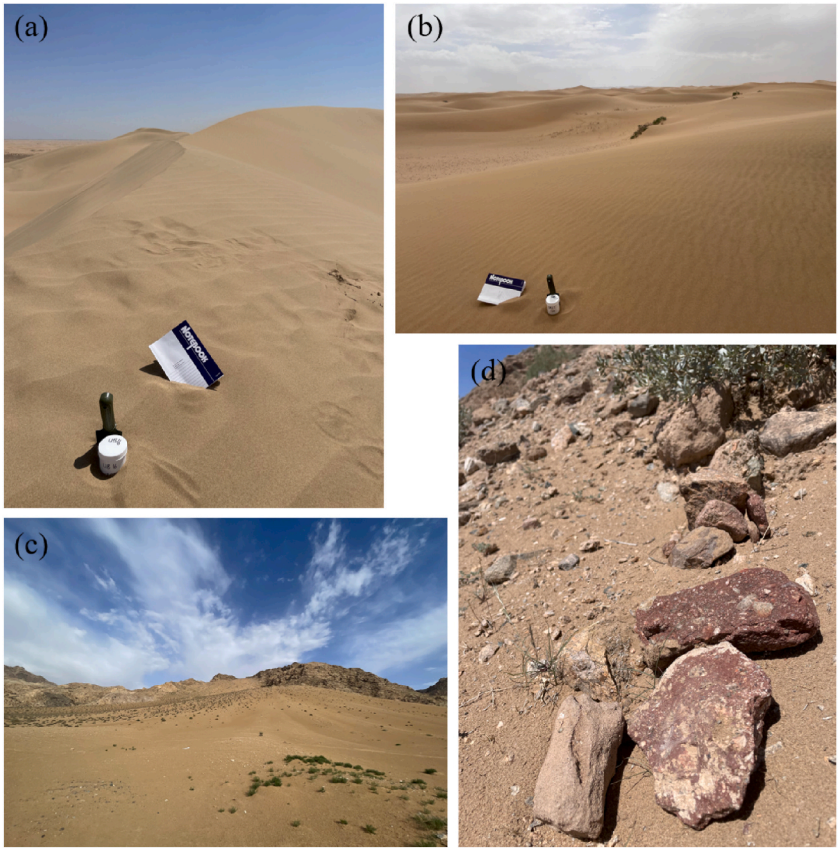

Fig. 2. Landscapes of the sampling sites. (a) Dune sands in the northern UBD. (b) Dune sands in the YD. (c) Sand cascade between the LM and the northern UBD. (d) LM bedrock detritus.

suggested by previous studies include the bedrocks of the LM, HM [7,17], and HLM [8]; the exposed bedrocks within the desert [17]; the eolian transport from the BJD [10,16,8] and deserts to the northwest of the HM [8]; and the Gobi sediments to the west [8,17]. The sediment source fingerprinting (SSF) method can provide quantitative information about the provenance of sediments [18]; however, the primary sources identified by each study differed, and the calculated proportion from bedrock detritus in surrounding mountains seems too high in SSF-based studies [8,19]. For example, Li et al. [19] concluded that 68 % of <125 μm fine sands were sourced from the LM, outnumbering the eolian transport from the YD and the local paleo-lacustrine sources. Chen et al. [8] also supported a high proportion of contribution from surrounding mountains; but their sampling sites were concentrated in the southern UBD, which may underestimate contributions from the YD and BJD to the northern UBD via the north rapidly expanding sand belt [5]. Moreover, there is a significant gap in our understanding of how bedrock in surrounding mountains weathered and produced particles overwhelmingly biased to very fine grains, which only account for a minor component in sand seas. In field research, we observed eolian sand transport directly climbing over the LM into the UBD, and forming 100–200 m wide sand cascades (Fig. 2c). Therefore, it is necessary to investigate and reevaluate the contribution of eolian sands from the YD and other potential sources, such as the BJD, to the northern UBD.

The research of tracing eolian sand provenance benefited from the booming of instrumental technologies since the late 20th century. Previous study approaches include magnetic susceptibility parameters [20,21], grain size parameters [22,23], OSL sensitivities [24,25], elemental [19,26–28], and isotopic geochemistry [29–31]. Among these methods, rare earth elements (hereafter referred to as REE) provide a powerful approach to tracing the source areas of sediments. REEs are a group of chemical elements, including scandium (Sc), yttrium (Y), and 15 lanthanide elements, as defined by the International Union of Pure and Applied Chemistry (IUPAC). All REEs exist in natural minerals at 10^2–10^3 ppm levels, but the abundance of Promethium (*Pm*) is ultra-low due to the absence of long-lived isotopes [32]. Sedimentary REE compositions are typically identical to their parent rocks, with little fractionation during erosion, transport, and sedimentary processes [33].

The sands with different grain size fractions usually have various sources and transport processes [28]. The coarser grains originate primarily from proximal environments, are predominantly mobilized through the channel system, and move more slowly [18]. In this study, we focused on the <125 μm fine fraction because fine sands are readily transported by wind over long distances, making them more sensitive to indicate external inputs from the BJD and the YD. We collected samples of surface sediments in the northern UBD and YD, as well as bedrock detritus in the LM piedmont, analyzed their REE contents in <125 μm fine fraction, and compared the REE characteristics with other potential sources and the southern UBD published by recent studies, in order to investigate the contribution of eolian sands from potential source areas to the northern UBD through the handclasp-shaped sand belts, reminding the role and threaten of sand belts as passages for eolian sand transport, and provide background knowledge for desertification combating in the farming-pastoral transitional zone in northwest China.

2. Materials and methods

2.1. Study area

The UBD is located southeast of the AP, Inner Mongolia, with a total area of approximately 11000 km^2 (Fig. 1a). The UBD is on the western boundary of the East Asian Summer Monsoon and within the transition zone between China's arid and semi-arid climate. The UBD is a part of the Hetao Basin, a Cenozoic fault basin surrounded by the Ordos Plateau [16]. The Quaternary paleo-lacustrine deposits are extensively distributed in the northern UBD [11]. The southern UBD is characterized by ~100 m high pyramid dunes and mega dunes [12]. The Jilantai Salt Lake and low dunes are distributed in the western region. The UBD has a continental climate, the annual precipitation ranges from 90 to 140 mm, with ~80 % occurring in summer, and the annual evaporation is 2240 mm [34].

The YD is located west of the LM, connecting the BJD in the northwest and the UBD in the east. The elevation of the YD decreases from west to east, with a total area of 5600 km^2. The majority of the dunes in the YD are mobile dunes (80 %), formed by barchan chains and barchan ridge dunes up to 50 m in height. The climate of the YD is extremely dry, with annual precipitation and evaporation of 70–150 mm and 2800–3600 mm, respectively [35]. There are no rivers flowing through the YD desert or the neighboring areas. Most surface sediments in the YD are eolian sands transported from upwind directions. There are two sand belts connecting the YD with the UBD: the north branch is located between the LM and the HM, and invades into the northern UBD; while the south branch is located across the HM and intrudes into the southern UBD around the Jilantai Salt Lake [5,36].

As a potential sediment source area for the YD and UBD, the BJD is China's second-largest mobile desert, located northwest of the AP. The BJD is surrounded by the GAM to the north, the Beishan Mountains (BM) and Heihe River (HR) to the west, the QM and HR to the south, and the Yabulai Mountain (YM) to the southeast (Fig. 1b). The BJD connected with YD in the east and TD to the southeast. The alluvial and lacustrine plains associated with the HR are distributed to the north and west [37]. The mega-dunes in the BJD are the tallest on Earth, with some giant transverse dunes as high as ~500 m [38], and mobile dunes cover approximately 80 % of the BJD [39,40]. The BJD has a typical continental climate; the Westerlies and the northwesterly winter monsoon controlled the eolian transport to the YD and TD [19]. The fine sand in the BJD has a mixed provenance from the QM and GAM, while the coarse fraction is mainly sourced from fluvial and Gobi sediments derived from the QM [19,28,41]. The latest research concluded that the Ejin Gobi sediments to the west were the primary source of sand for the BJD, while HR fluvial sediments were the secondary source [42].

2.2. Sample collection

The samples were collected during July 2022, including eighteen eolian sand samples from the northern UBD (UBD1-UBD18), six

eolian sand samples from the eastern YD (YD1-YD6), and two bedrock detritus samples from the southern slope of the LM (LM1 and LM2). The sampling locations for this study are depicted in Fig. 1a. The sampling sites of the UBD were evenly spaced and covered the northern half of the UBD. The six YD sampling sites were separated from the UBD by the LM and were located along a zonal transect of the eastern YD. Each sample was collected from sand crests of the top 3 cm within a 50 × 50 cm area. Bedrock samples were collected at piedmont sand cascades. Fig. 2a - d depicts landscape photographs of representative sampling sites.

2.3. Sample analyses

The <125 μm fractions of fine sands were separated by dry sieves. Before digestion and analysis, the bedrock detritus and the sieved fine sands were milled to a fineness of >200 mesh. The detailed sample digestion and pre-treatment procedures were as follows: (1) Sample powder (200 mesh) was dried in an oven at 105 °C for 12 h; (2) 50 mg sample powder was accurately weighed and placed in a Teflon bomb; (3) 1 ml HNO_3 and 1 ml HF were slowly added into the Teflon bomb; (4) The Teflon bomb was placed in a stainless steel pressure jacket and heated at 190 °C in an oven for 24 h (5) After cooling, the Teflon bomb was opened and placed on a hotplate at 140 °C, evaporated to dryness, and then 1 ml HNO_3 was added and evaporated to dryness again; (6) 1 ml of HNO_3, 1 ml of MQ water and 1 ml internal standard solution of 1 ppm In was added, and the Teflon bomb was resealed and placed in the oven at 190 °C for >12 h; (7) The final solution was transferred to a polyethylene bottle and diluted to 100 g by the adding 2 % HNO_3.

The REE analysis of all samples was conducted on Agilent 7700e ICP-MS at the Wuhan SampleSolution Analytical Technology Co., Ltd., Wuhan, China. Blank and parallel samples, as well as three international rock standards of USGS reference materials BCR-2 (basalt), BHVO-2 (basalt), and RGM-2 (rhyolite) were used to monitor analytical accuracy. The software ICPMSDataCal was used to perform offline selection and integration of background and analyzed signals, time-drift corrections, and quantitative calibrations of trace-element analyses. The precision and accuracy of all measured samples were better than 5 %.

All of the REEs were normalized to chemical compositions of chondrite values recommended by Boynton [43], where the subscript ''N'' represents normalized REE. The anomalies of Eu and Ce were calculated as $Eu/Eu^* = Eu_N/(Sm_N \times Gd_N)^{1/2}$ and $Ce/Ce^* = Ce_N/(Sm_N \times Gd_N)^{1/2}$. The ∑REE, ∑LREE, and ∑HREE were regarded as the sum of REE concentrations of Lã Lu, Lã Eu, and Gd ~ Lu, respectively.

3. Results and discussion

3.1. REE concentrations and chondrite-normalized patterns

The REE concentrations ($\mu g \cdot g^{-1}$) of all samples are given in Table S1 of the supplementary materials. The summed ∑REE, ∑LREE, ∑HREE ($\mu g \cdot g^{-1}$), and other REE characteristic parameters are shown in Table 1. The REEs from La to Nd have more considerable variations in contents, with variation coefficients (ratio of standard error and average value) > 0.5, while concentrations of Sm ~ Lu have minor fluctuations. The ∑REE of surface sediments in the northern UBD range between 47.4 and 199.3 $\mu g\ g^{-1}$, with an average of

Table 1
REE characteristic parameters of all samples.

Region	Sample	∑REE	∑LREE	∑HREE	LREE/REE	δCe	δEu	$(La/Sm)_N$	$(Gd/Yb)_N$	$(Gd/Er)_N$	$(La/Gd)_N$
UBD	UBD1	82.99	74.22	8.77	0.894	0.98	0.76	3.81	1.44	1.43	6.09
	UBD2	116.07	102.67	13.40	0.885	0.98	0.70	3.70	1.42	1.42	5.51
	UBD3	47.39	41.96	5.42	0.886	0.98	0.92	3.74	1.33	1.36	5.73
	UBD4	122.54	109.47	13.07	0.893	0.99	0.74	3.69	1.46	1.47	5.69
	UBD5	109.06	96.21	12.84	0.882	1.03	0.74	3.57	1.35	1.33	5.34
	UBD6	146.48	130.07	16.41	0.888	0.99	0.65	3.79	1.30	1.35	5.77
	UBD7	125.44	111.99	13.45	0.893	0.98	0.69	3.83	1.38	1.42	5.95
	UBD8	64.57	56.97	7.60	0.882	0.97	0.86	3.65	1.42	1.39	5.35
	UBD9	140.05	121.80	18.24	0.870	0.98	0.67	3.43	1.27	1.29	4.97
	UBD10	170.72	150.17	20.55	0.880	1.01	0.58	3.58	1.23	1.35	5.26
	UBD11	199.26	177.31	21.95	0.890	0.98	0.54	3.50	1.38	1.49	5.44
	UBD12	79.23	70.18	9.05	0.886	0.97	0.78	3.77	1.48	1.46	5.48
	UBD13	98.75	87.47	11.28	0.886	0.98	0.74	3.60	1.52	1.47	5.32
	UBD14	152.26	134.93	17.33	0.886	0.99	0.60	3.75	1.40	1.45	5.52
	UBD15	143.31	127.68	15.63	0.891	1.00	0.70	3.91	1.27	1.35	6.00
	UBD16	100.71	88.97	11.73	0.883	0.99	0.75	3.61	1.25	1.30	5.57
	UBD17	79.96	70.93	9.03	0.887	0.99	0.77	3.71	1.29	1.37	5.74
	UBD18	142.65	125.44	17.21	0.879	1.01	0.67	3.48	1.21	1.28	5.42
YD	YD1	53.31	47.17	6.14	0.885	1.00	0.96	3.67	1.30	1.33	5.66
	YD2	132.17	113.63	18.54	0.860	1.05	0.69	2.98	1.02	1.14	4.59
	YD3	58.64	51.40	7.24	0.876	0.98	0.89	3.50	1.25	1.34	5.16
	YD4	96.33	84.43	11.91	0.876	1.01	0.76	3.15	1.20	1.29	5.03
	YD5	56.58	49.79	6.79	0.880	0.98	0.90	3.44	1.32	1.31	5.29
	YD6	82.16	72.60	9.55	0.884	1.04	0.76	3.43	1.20	1.31	5.49
LM	LM1	361.07	347.89	13.18	0.964	0.99	0.84	6.71	3.82	2.79	14.01
	LM2	63.06	59.35	3.70	0.941	1.03	0.58	4.39	1.84	2.02	9.50

114.5 μg g^{-1}. The ∑REE of six samples in the YD range between 53.3 and 132.2 μg g^{-1}, with an average of 79.9 μg g^{-1}, slightly lower than the UBD samples. The ∑REE of LM1 and LM2 are 361.1 and 63.1 μg g^{-1}, respectively. The ∑LREE/∑REE ratios of LM bedrock (95.2 %) are higher than those in the UBD (88.6 %) and the YD (87.7 %).

The ∑REE values in this study are identical to those of sediments in the <125 μm fraction from the UBD (65.6–174.6 μg g^{-1}, averaged of 110.4 μg g^{-1}) reported by Ref. [8], but they are lower than the fine fraction (<64 μm) of sediments from the Qaidam Basin Desert (QBD), the BJD, and the TD [44]. The differences in ∑REE between UBD and YD result from differences in particle size distribution rather than sediment provenance since the REE contents are highly sensitive to grain size, i.e., fine fractions often have significantly greater concentrations than coarse fractions [33]. The chondrite-normalized elemental ratios of $(La/Yb)_N$ and $(Gd/Yb)_N$ are proper REE parameters to reflect the enrichment of LREE and depletion of HREE, respectively. The average $(La/Yb)_N$ ratios for the UBD and YD are 7.53 and 6.35, whereas the average $(Gd/Yb)_N$ ratios for the UBD and YD are 1.35 and 1.22, respectively. These results show that the UBD samples are more enriched in LREE and depleted in HREE.

The chondrite-normalized REE pattern of surface sediments in the UBD and YD are both characterized by steep LREE, negative Eu anomalies, and flat HREE (Fig. 3a and b), similar to fine sands in the southern UBD [8], BJD [19,41], the Ordos Dessert (Mu Us Sandy Land and Hobq Desert) [30,45], and sedimentary rocks [33]. The only exception is LM1 bedrock, with much higher LREE and a right cline HREE. In principle, REEs in the oceanic crust have little differentiation and generally exhibit a flat REE pattern; in contrast, in felsic rocks of the upper continental crust, LREE are relatively enriched, and the HREE are depleted [46]. The uniformity of chondrite-normalized REE patterns in sedimentary rocks results from various provenance components from the upper crust, and the average sedimentary REE pattern is identical to the average upper crust REE pattern [33]. Hence, surface sediments in the UBD and YD have REE patterns that indicate their origin in felsic rocks but are unable to distinguish them from other eolian sand and dust sources in northern China.

La, Gd, and Yb were chosen to represent REEs from light to heavy. The La-Gd-Yb ternary diagram of all samples in this study, together with results of previous studies in the UBD, BJD, and other potential sources, are shown in Fig. 4a. In the La-Gd-Yb plots, the UBD and YD fall in between the QM and GAM groups and depart from the southern UBD and HM, which have higher abundance in La but lower abundance in Gd.

Sc behaves similarly to the REEs during sedimentary processes, and the ratios of Sc to other REEs provide useful information about sediment provenance [33]. In the ternary diagram of Y-Sc-Ce (Fig. 4b), the distribution of UBD and YD samples are almost identical, partially overlapping with BJD, but completely independent from any other sources. The BJD, on the other hand, shows a wider distribution in both ternary plots and overlaps with sources other than the HM.

3.2. Eu and Ce anomalies

Eu can exist in a divalent state and has a similar ionic radius to Sr, allowing it to replace Sr in Ca-plagioclase. A negative Eu anomaly observed in the Upper Continental Crust (UCC) suggests that intra-crustal differentiation plays a dominant role in controlling the distribution of elements [33]. In general, basalts are indicative of a predominantly mantle-derived origin without any Eu anomaly [47]. Conversely, felsic rocks from the UCC and their derived sedimentary rocks exhibit depletions in Eu relative to Sm and Gd, thereby displaying negative Eu anomalies. Hence, discrepancies in Eu/Eu* can reflect the provenances of eolian sediments [28,46]. The bivariate plots of Eu/Eu* and normalized REE ratios can provide background knowledge about sediment provenance. For example, the plots of $(La/Yb)_N$ vs. Eu/Eu* were applied to illustrate sediment provenances in northern China [28,48,49]. Ferrat et al. [44] summarized that studies of Asian dust present chondrite-normalized REE ratios of $(La/Yb)_N$ ~10 and Eu/Eu* ~0.65 [50–53].

In this study, the Eu/Eu* ratios of all samples exhibit a wide range of variation (0.54–0.96), which is comparable to the variation range in the UCC [54], sedimentary rocks [33], and Asian dust [44]. As significant potential sources of sediment in the BJD and UBD, the sediments from QM (0.82) and GAM (0.61) exhibit distinct endmembers based on their Eu/Eu* ratios, while the Eu/Eu* ratios of BJD, YD, and UBD fall within intermediate ranges. The Eu/Eu* vs. ∑REE plots (Fig. 5a) present an inverse correlation, while the LM

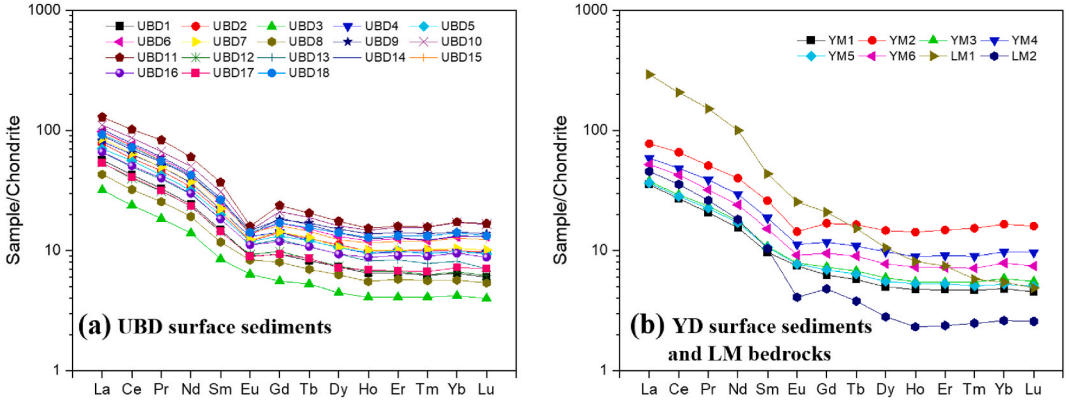

Fig. 3. Chondrite-normalized REE distribution patterns (spider diagram) of sediments in (a) UBD, (b) YD, and LM bedrocks.

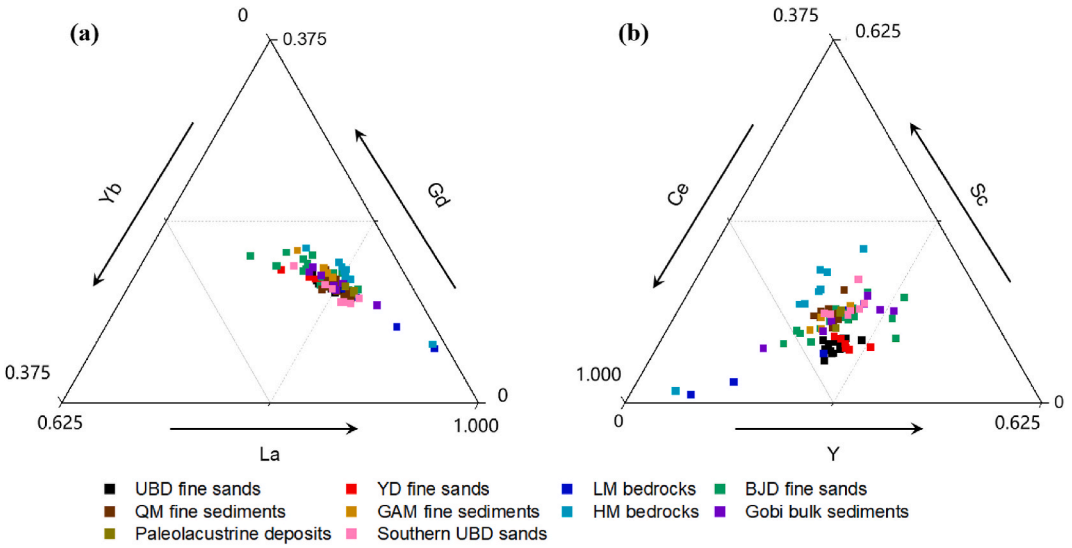

Fig. 4. Ternary diagram of (a) La-Gd-Yb and (b) Y-Sc-Ce. The REE data of LM, southern UBD, HM, Gobi, and paleo-lacustrine deposits are from Ref. [7]; The data of BJD, QM, and GAM are adopted from Ref. [19].

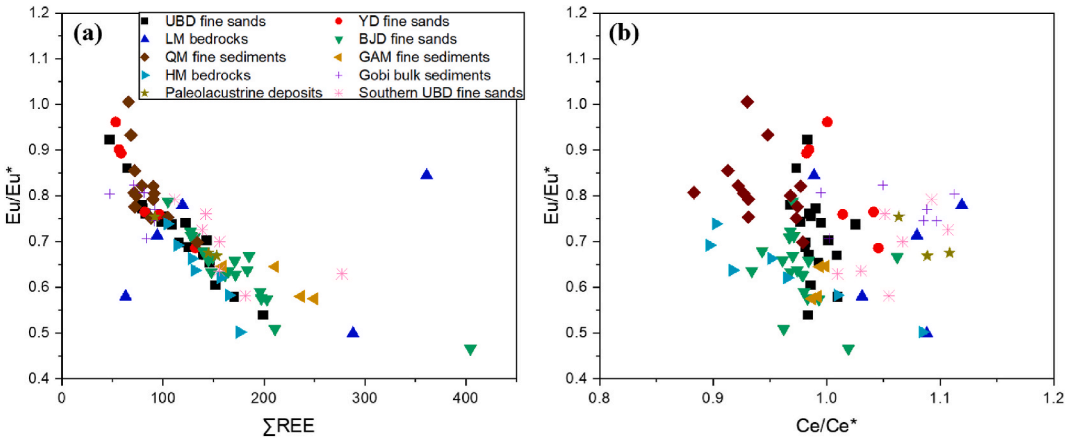

Fig. 5. Bivariate plots of (a) Eu/Eu* vs. ∑REE and (b) Eu/Eu* vs. Ce/Ce*. Data sources are the same as in Fig. 4.

bedrocks display a discrete pattern. In both bivariate plots, the YD barely overlapped with the HM and GAM, indicating that these mountains are not the YD's main sediment source areas.

Ce is more sensitive to sedimentary redox environments than other REEs. The trivalent Ce is soluble under anoxic conditions and becomes insoluble in water at low temperatures when oxidized to tetravalent Ce. In contrast, all other REEs exist exclusively in a trivalent oxidation state. Thus, the Ce anomalies in sediments are indicators of local redox conditions in paleosols, lakes, and marine environments, where negative Ce anomalies usually result from settings of oxidic, higher pH values, and lower organic material contents [55–57]. Most samples of the UBD and YD did not show Ce anomalies, with Ce/Ce* range between 0.97 and 1.05, within the scope of the fine sands in the BJD (0.94–1.08) [8], indicating dry environments in the BJD, YD and northern UBD. By contrast, the QM sediments and HM bedrocks have negative Ce anomalies.

However, the southern UBD sands, the paleo-lacustrine deposits, and the LM bedrocks show slightly positive Ce/Ce* (Fig. 5b). Most of the modern UBD area was covered by the Jilantai-Hetao Mega-paleolake during the late Quaternary, lasting until ~90 ka ago [16], and the abundant nutrient supply under warm climate conditions may have resulted in redox conditions [58]. The slightly positive Ce anomalies observed in the paleo-lacustrine deposits may be derived from sedimentary redox conditions during the Mega-paleolake periods, mixed with other sources of sediments when dunes began to form, and finally inherited by the southern UBD fine sediments. In the plots of Eu/Eu* vs. Ce/Ce* (Fig. 5b), the southern UBD fields largely overlapped with the LM bedrocks, Gobi sediments, and paleo-lacustrine deposits, supporting the conclusion that they are the primary source regions for the southern UBD [7,17].

3.3. Provenance and transport processes of fine sands in the northern UBD

Among the local and peripheral source areas, we assume the bedrocks of HM and LM, the paleo-lacustrine deposits, and the Gobi sediment to the west as potential sources of fine eolian sands for the northern UBD. The HLM locates downwind from the UBD and is not likely to be a primary source of sediments in the northern UBD [17]. As shown by sand drift potentials for meteorological stations of the Ejina, Guaizihu, Bayin Mod, and Hailisu (Fig. 1b), the BJD is a potential distant/indirect source of fine sand to the UBD via the sand belts through the YD [16]. Moreover, based on historical Google Earth images during 2003–2013, the averaged dune mitigation rate and direction in the YD were calculated to be 9.1 m/yr and 118.3°, respectively [7], supporting the eolian transport from the YD to the downwind northern UBD. Although the LM blocked most of the direct eolian transport, sand transport through the sand cascade was observed. A previous study concluded that the development of dune landforms in these sand belts connecting the YD and UBD occurred between 1000 and 2000 years ago [10], coinciding with the rapid eolian sand deposition in the UBD [9].

Tracking back to the upstream of sediments in AP deserts, the eolian sands in the BJD are derived from the alluvial/fluvial fan formed by the HR, which drains the QM under an arid Pleistocene climate [37]. The GAM locates in the upwind direction of the BJD, also contributes sediments to the BJD. Therefore, both the QM and GAM are potential source areas for fine sands in the BJD [19]. Consequently, the QM, GAM, and BJD may constitute the majority of distant/indirect sediment sources for the YD and the northern UBD. Therefore, we conducted a comparative analysis of the compositions and ratios of REE in eolian sands from the northern UBD and YD studied here with those from potential sources previously reported by other researchers. The REE data include distant/indirect potential sources from the fine sands in the BJD, alluvial sediment of HR originating from the QM, fine piedmont sediments of the GAM [19], as well as the proximal/direct sources from bedrock detritus of the HM and LM, the Gobi sediments to the west of the UBD, and the paleo-lacustrine deposits in the UBD [7]. The REE of southern UBD's fine sands were also compared to those of the northern UBD to determine if they originated from different source areas. All REE data employed in the literature were derived from the <125 μm fraction, consistent with our samples in the northern UBD and YD.

Since the Eu and Ce anomalies and normalized REE patterns are insensitive to differentiate the delicate difference between each source, we compared the chondrite-normalized REE ratios of $(Gd/Er)_N$, $(La/Gd)_N$, $(La/Sm)_N$, and $(Gd/Yb)_N$ in the UBD and YD, with potential source areas (Fig. 6a–c), to examine the genetic linkage and differences of eolian sands between the UBD and potential sources listed above. The ratios of Y/Tb_N, $(La/Yb)_N$, and $Y/\sum REE$ were also applied in the comparison (Fig. 7), as they are reported to be insensitive to the grain size effect in deserts of China [44]. The detailed analysis for each potential source is presented below.

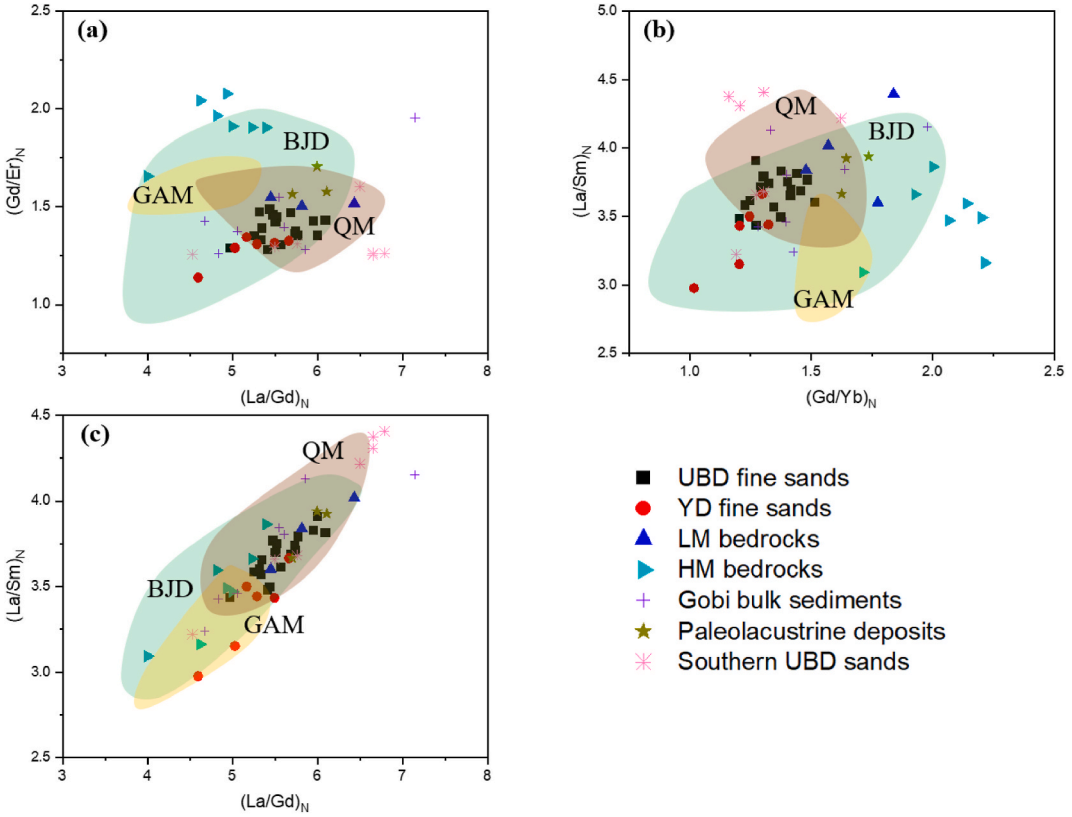

Fig. 6. Bivariate plots of (a) $(Gd/Er)_N$ vs. $(La/Gd)_N$, (b) $(La/Sm)_N$ vs. $(Gd/Yb)_N$, and (c) $(La/Sm)_N$ vs. $(La/Gd)_N$. The fields of BJD, QM, and GAM are represented in colors of green, brown, and yellow, respectively. The boundaries of the colored fields were delineated based on the peripheral contours of their respective scatter data points at the same coordinate scale. Data sources are the same as in Fig. 4.

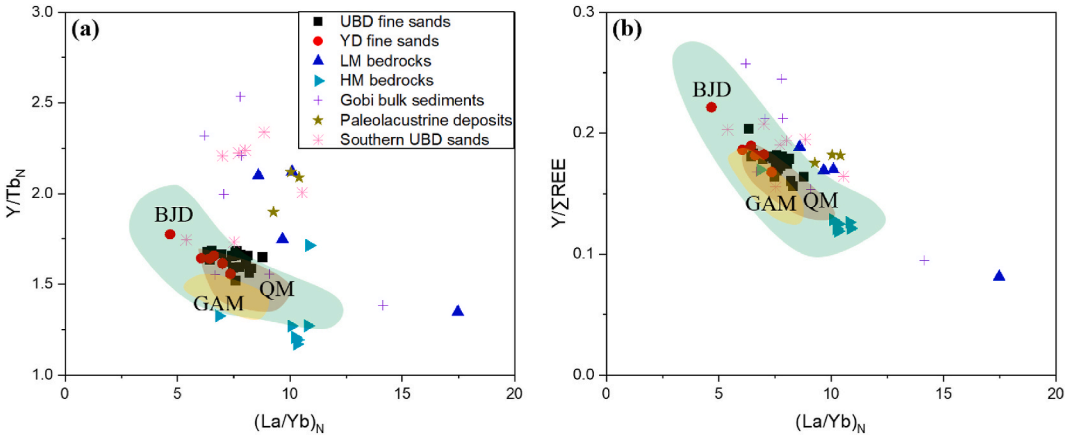

Fig. 7. Bivariate plots of (a) Y/Tb_N vs. $(La/Yb)_N$ and (b) $Y/\sum REE$ vs. $(La/Yb)_N$. The fields of BJD, QM, and GAM are represented in colors of green, brown, and yellow, respectively. The boundaries of the colored fields were delineated based on the peripheral contours of their respective scatter data points at the same coordinate scale. Data sources are the same as in Fig. 4.

The northern margin of the Tibetan Plateau (NTP) represented by the QM and the Central Asian Orogen (CAO) represented by the GAM have been suggested as two ultimate material sources of Asian dust [1]. The ultimate source of the BJD is also composed of the NTP and CAO, although the detailed proportions have been debated for years [19,28,42]. In Figs. 6 and 7, the BJD shows widely dispersed patterns, while the QM, GAM, UBD, and YD fall within or close to the BJD field. The slopes of the $Y/\sum REE$ vs. (La/Yb)N relationship (Fig. 7b) were found to be identical for both the BJD and YD samples, following the observations that eolian sand in the YD was continuously recharged from the BJD through sand belts, reported by a recent study [6].

Although some of the QM sediments have high $(Gd/Er)_N$ and $(La/Sm)_N$ ratios, the majority of QM sediments overlap with the BJD, UBD, and YD. Compared to the YD, the UBD are closer to the QM, especially in plots of $(La/Sm)_N$ vs. $(Gd/Yb)_N$ and $(La/Sm)_N$ vs. $(La/Gd)_N$ (Fig. 6b and c). It is somewhat unexpected that the YD is geographically closer to the BJD and QM than the UBD, and its REE proxies were supposed to be closer to the BJD or QM. An explanation is that other external sources from the north contribute to the YD; for example, the YD partially overlaps with the GAM in plots of $(La/Sm)_N$ vs. $(La/Gd)_N$ (Fig. 6c), indicating eolian transport from the GAM and Southern Mongolian Gobi. The partial overlap between the QM and the southern UBD also indicates possible direct transport of fine-grained sand from QM to the UBD by the Westerlies. It is important to note that the samples representing QM endmembers consist of alluvial sand from the HR, which may not be completely identical to bedrocks from the QM and could have undergone some degree of mixing with sediments exhibiting GAM signals.

As a minor source of fine-grained sands in the BJD, the REE ratios for GAM in all plots are distinct from those found in the UBD, suggesting that the piedmont sediments in the GAM are not the primary sources of the UBD. The Westerlies and the winter monsoon dominate eolian transport processes in these regions, and sand drift potential points to the direction from the Southern Mongolian Gobi to the YD and UBD. Geographically, the intervening mountains, specifically the LM to the north of the UBD, obstructed the direct eolian transport pathway of sediments from the GAM piedmont by the northwestern winter monsoon, and the YD acts as a buffer zone or mixing vessel for eolian sand from the west and northwest. Therefore, the main distant source areas of fine-grained sands in the northern UBD are the QM and BJD, whereas the GAM is a minor source for the northern UBD. Still, it is worth noting that the YD is closer to the GAM in plots of $(La/Sm)_N$ vs. $(La/Gd)_N$, Y/Tb_N vs. $(La/Yb)_N$, and $Y/\sum REE$ vs. $(La/Yb)_N$, indicating that sediments from the GAM piedmont were transported to the YD, supported by the resultant sand drift potential for the Hailisu meteorological station (Fig. 1b).

A previous study estimated that approximately 68 % of the fine-grained sands in the UBD originated from the LM bedrock [7]. However, in the bivariate REE plots of Figs. 6 and 7, the LM is observed to be distributed outside the UBD range. Based on our data and previous research, it can be inferred that the composition of LM bedrock is highly heterogeneous. Some outliers even exceed the scale range in our REE plots. Furthermore, we only observed overlap with UBD in plots of $(La/Sm)_N$ vs. $(La/Gd)_N$ (refer to Fig. 6c). Compared to the northern UBD samples in this study, the southern UBD samples have overlapped with the LM in plots of Y/Tb_N vs. $(La/Yb)_N$ and $Y/\sum REE$ vs. $(La/Yb)_N$, indicating the contribution from the LM may be overwhelmed by signals from the YD. Therefore, we do not consider the LM to be a primary source of fine-grained sand in the northern UBD. Likewise, the HM to the south of the YD and the west of the UBD is not a primary source of fine sands in the northern UBD. The HM in all REE plots barely overlaps with the field of UBD and YD and even falls out of the southern UBD field, despite a more concentrated distribution than the LM. However, in plots of Y/Tb_N vs. $(La/Yb)_N$ (Fig. 7a), the several data points distributed to the margin and outside of the BJD field are oriented towards the LM direction, indicating that LM may have a minor contribution to the northern UBD. According to these results, neither the LM nor the HM is the major source area of fine-grained sands in the northern UBD.

The Gobi sediments west of the UBD show widely dispersed patterns in most REE plots and can simultaneously overlap with the YD, northern, and southern UBD. The wide range of REE ratios suggests that Gobi sediments are very heterogenous, receiving detrital deposits from surrounding mountains. The paleo-lacustrine deposits are widespread in the UBD, and previous studies have confirmed

that they are one of the main sources of eolian sands in the UBD [7,8,17]. However, the paleo-lacustrine deposits in REE plots did not fall within the northern UBD in this study but have largely overlap with the southern UBD, especially in plots of Y/Tb_N vs. $(La/Yb)_N$ and $Y/\sum REE$ vs. $(La/Yb)_N$. This observation suggests that the paleo-lacustrine deposits are one of the main sources for the southern UBD. It is worth noting that the northern and southern UBD in REE plots has hardly overlapped with each other, indicating their different provenances and sediment transport processes. Geographically connected by handclasp-shaped sand belts, the sediments in the northern UBD have REE genetic linkage close to the YD, BJD, and QM. In contrast, the surface sediments in the southern UBD contain a mixture of the LM bedrocks, paleo-lacustrine deposits, Gobi sediments, and minor contributions from the BJD and QM.

The heterogeneity and limited sample size of bedrock detritus in the LM impede further interpretation of contributions from this region in our study. Meanwhile, the insufficient understanding of REE proxies concerning mineralogy, weathering, and transportation processes remains to be clarified. Future research should further identify the specific REE endmembers to better constrain the contribution from surrounding mountains, explore the physical and chemical mechanisms behind these REE proxies, and examine the REE-based results with other tracers such as the Sr–Nd isotopes.

4. Conclusion

In this study, we analyzed the REE contents present in eolian sands with a particle size of less than 125 μm from the northern regions of UBD and YD. Furthermore, we compared their REE characteristics with those found in sediments and bedrock from potential source areas. The following conclusions were drawn:

(1) The sediments in the UBD and YD exhibit enrichment of LREE, with chondrite-normalized patterns characterized by pronounced LREE enrichment, negative Eu anomalies, and relatively constant HREE concentrations. These REE distribution patterns of eolian sands are consistent with other deserts in China. The Eu/Eu* ratios of all samples exhibit a wide range of variation (0.54–0.96), which is consistent with the UCC and Asian dust. The sedimentary Eu/Eu* values in QM (0.82) and GAM (0.61) represent distinct endmembers, while YD and UBD display intermediate values. The Ce/Ce* range between 0.97 and 1.05, reflecting the dry climates of the YD and northern UBD.

(2) The QM and BJD are the primary sources of fine-grained sands in the northern UBD via the YD, whereas the LM blocks the direct contribution from the GAM. The QM-HR-BJD-YD-UBD is the primary route for the transport of fine-grained sands by the Westerlies and winter monsoons. The LM serves as a minor contributor of sands in the UBD, however, its heterogeneity and limited sample size impede further assessment of its impact on the UBD. The primary sources of fine-grained sands in the southern and northern UBD exhibit significant differences.

Our findings indicate that the transportation of fine-grained sands over long distances through sand belts is a significant process in the northern UBD, which differs from the southern UBD in terms of both sediment origin and transport mechanism. Furthermore, urgent attention must be paid to the handclasp-shaped connecting zones among the Alxa Deserts, and measures aimed at reversing the expanding trend of sand belts should be implemented in future efforts to combat desertification, rather than being confined solely to local environmental restoration.

Data availability statement

All data generated or analyzed throughout this study are included in this published article and supplementary materials.

CRediT authorship contribution statement

Weiyuan Kong: Conceptualization, Data curation, Formal analysis, Funding acquisition, Investigation, Methodology, Writing - original draft, Writing - review & editing. **Shangzhe Zhou:** Investigation, Methodology. **Guipeng Cui:** Data curation, Formal analysis. **Pan Gao:** Data curation, Formal analysis. **Shuai Li:** Investigation. **Qi Lu:** Conceptualization, Funding acquisition.

Declaration of competing interest

The authors declare that they have no known competing financial interests or personal relationships that could have appeared to influence the work reported in this paper.

Acknowledgment

This research was funded by the National Natural Science Foundation of China (No. 32201635 and 32101592), Central Public-Interest Scientific Institution Basal Research Fund of China (No. CAFYBB2021ZD003), Science & Technology Fundamental Resources Investigation Program (No. 2022FY202300 and 2022FY202301).

Appendix A. Supplementary data

Supplementary data to this article can be found online at https://doi.org/10.1016/j.heliyon.2023.e22904.

References

[1] J. Chen, G. Li, Geochemical studies on the source region of Asian dust, Sci. China Earth Sci. 54 (9) (2011) 1279–1301.
[2] X. Wang, F. Chen, E. Hasi, J. Li, Desertification in China: an assessment, Earth Sci. Rev. 88 (3–4) (2008) 188–206.
[3] B.A. Bryan, L. Gao, Y. Ye, X. Sun, J.D. Connor, N.D. Crossman, M. Stafford-Smith, J. Wu, C. He, D. Yu, China's response to a national land-system sustainability emergency, Nature 559 (7713) (2018) 193–204.
[4] R. Arimoto, Eolian dust and climate: relationships to sources, tropospheric chemistry, transport and deposition, Earth Sci. Rev. 54 (1–3) (2001) 29–42.
[5] J. Tan, W. Yang, K. Qi, Y. Tian, J. Mi, L. Li, S. Sun, Status investigated and countermeasure about "burst" and "handclasp" of four desert in alashan league, Journal of Inner Mongolia Forestry Science and Technology (3) (2006) 4–7 (in Chinese with English abstract).
[6] W. Sun, X. Gao, J. Lei, Shaping effects of sand flow channels on aeolian geomorphology–a case study of the Badain Jaran, Tengger, and Ulan Buh Deserts, northern China, Catena 214 (2022), 106255.
[7] Z. Li, X. Yu, Q. Chen, S. Dong, C. Zhang, Quantitative tracing of provenance for modern eolian sands with various grain size fractions in the Ulan Buh Desert, northwestern China, Catena 217 (2022), 106487.
[8] G. Chen, A. Liang, Z. Dong, W. Shi, C. Li, W. Nan, T. Shao, Quantification of the aeolian sand source in the Ulan Buh Desert using the sediment source fingerprinting (SSF) method within MixSIAR modelling framework, Catena 219 (2022), 106579.
[9] R. Hou, W. Yu, Archaeological discoveries and environmental changes in the ulan buhe desert, Archaeology 2 (1973) 5–7 (in Chinese with English abstract).
[10] Y. Fan, F. Chen, T. Fan, H. Zhao, L. Yang, Sedimentary documents and Optically Stimulated Luminescence (OSL) dating for formation of the present landform of the northern Ulan Buh Desert, northern China, Sci. China Earth Sci. 53 (11) (2010) 1675–1682.
[11] H. Zhao, G. Li, Y. Sheng, M. Jin, F. Chen, Early–middle Holocene lake-desert evolution in northern ulan Buh Desert, China, Palaeogeogr. Palaeoclimatol. Palaeoecol. 331 (2012) 31–38.
[12] X. Chun, F. Chen, Y. Fan, D. Xia, H. Zhao, Formation of ulan Buh Desert and its environmental changes during the Holocene, Front. Earth Sci. China 2 (3) (2008) 327–332.
[13] T. Jia, S. Yin, Geomorphic evolution in northern ulan Buh Desert in the Holocene, Sci. Geogr. Sin. 24 (2004) 217–221 (in Chinese with English abstract).
[14] G. Li, M. Jin, X. Chen, L. Wen, J. Zhang, D. Madsen, H. Zhao, X. Wang, T. Fan, Y. Duan, Environmental changes in the Ulan Buh Desert, southern Inner Mongolia, China since the middle Pleistocene based on sedimentology, chronology and proxy indexes, Quat. Sci. Rev. 128 (2015) 69–80.
[15] G. Li, M. Jin, L. Wen, H. Zhao, D. Madsen, X. Liu, D. Wu, F. Chen, Quartz and K-feldspar optical dating chronology of eolian sand and lacustrine sequence from the southern Ulan Buh Desert, NW China: implications for reconstructing late Pleistocene environmental evolution, Palaeogeogr. Palaeoclimatol. Palaeoecol. 393 (2014) 111–121.
[16] F. Chen, G. Li, H. Zhao, M. Jin, X. Chen, Y. Fan, X. Liu, D. Wu, D. Madsen, Landscape evolution of the ulan Buh Desert in northern China during the late quaternary, Quat. Res. 81 (3) (2014) 476–487.
[17] C. Zhang, Z. Li, Q. Chen, S. Dong, X. Yu, Q. Yu, Provenance of eolian sands in the Ulan Buh Desert, northwestern China, revealed by heavy mineral assemblages, Catena 193 (2020), 104624.
[18] D.E. Walling, The evolution of sediment source fingerprinting investigations in fluvial systems, J. Soils Sediments 13 (10) (2013) 1658–1675.
[19] B. Li, Q. Feng, Z. Li, F. Wang, T. Yu, X. Guo, H. Xi, Geochemical characteristics of surface aeolian sand in the Badain Jaran Desert, northwestern China: implications for weathering, sedimentary processes and provenance, Catena 219 (2022), 106640.
[20] L.P. Hällberg, T. Stevens, B. Almqvist, I. Snowball, S. Wiers, C. Költringer, H. Lu, H. Zhang, Z. Lin, Magnetic susceptibility parameters as proxies for desert sediment provenance, Aeolian Research 46 (2020), 100615.
[21] Q. Liu, Y. Sun, X. Qiang, R. Tada, P. Hu, Z. Duan, Z. Jiang, J. Liu, K. Su, Characterizing magnetic mineral assemblages of surface sediments from major Asian dust sources and implications for the Chinese loess magnetism, Earth Planets Space 67 (1) (2015) 1–17.
[22] Y. Zhang, X. Chun, H. Zhou, Grain size discriminant method for eolian and lacustrine sediments of deserts and it's environmental indication, J. Desert Res. 40 (5) (2020) 1–9 (in Chinese with English abstract).
[23] J. Song, X. Chun, The spatial variation and grain size character of different land cover types in the Ulanbuh Desert, J. Desert Res. 38 (2018) 243–251 (in Chinese with English abstract).
[24] T. Lü, J. Sun, J.K. Feathers, D. Sun, Spatiotemporal variations and implications of luminescence sensitivity of quartz grains on the Chinese Loess Plateau since the last interglaciation, Quat. Res. 99 (2021) 190–203.
[25] C. Zheng, L. Zhou, J. Qin, Difference in luminescence sensitivity of coarse-grained quartz from deserts of northern China, Radiat. Meas. 44 (5–6) (2009) 534–537.
[26] G. Wei, C. Zhang, Q. Li, H. Wang, R. Wang, Y. Zhang, Y. Yuan, Characterization of geochemical elements in surface sediments from Chinese deserts, Catena 220 (2023), 106637.
[27] X. Liang, Q. Niu, J. Qu, B. Liu, B. Liu, C. Zhang, T. Liu, Geochemical analysis of yardang strata in the Dunhuang Yardang National Geopark, Northwest China, and implications on its palaeoenvironment, provenance, and potential dynamics, Aeolian Research 40 (2019) 91–104.
[28] F. Hu, X. Yang, Geochemical and geomorphological evidence for the provenance of aeolian deposits in the Badain Jaran Desert, northwestern China, Quat. Sci. Rev. 131 (2016) 179–192.
[29] T.C. Rousseau, M. Roddaz, J.-S. Moquet, H.H. Delgado, G. Calves, G. Bayon, Controls on the geochemistry of suspended sediments from large tropical South American rivers (Amazon, Orinoco and Maroni), Chem. Geol. 522 (2019) 38–54.
[30] W. Rao, H. Tan, S. Jiang, J. Chen, Trace element and REE geochemistry of fine-and coarse-grained sands in the Ordos deserts and links with sediments in surrounding areas, Geochemistry 71 (2) (2011) 155–170.
[31] W. Rao, J. Chen, H. Tan, S. Jiang, J. Su, Sr-Nd isotopic and REE geochemical constraints on the provenance of fine-grained sands in the Ordos deserts, north-central China, Geomorphology 132 (3–4) (2011) 123–138.
[32] V. Balaram, Rare earth elements: a review of applications, occurrence, exploration, analysis, recycling, and environmental impact, Geosci. Front. 10 (4) (2019) 1285–1303.
[33] S.M. McLennan, Rare earth elements in sedimentary rocks: influence of provenance and sedimentary processes, Geochemistry and Mineralogy of Rare Earth Elements. Rev. Mineral. 21 (1989) 169–200.
[34] N. Wang, X. Chun, Research progress on the quaternary environmental evolution in the ulan Buh Desert, J. Desert Res. 42 (2022) 175 (in Chinese with English abstract).
[35] N. Liu, The Influence of Wind Forming on the Physical and Chemical Properties of the Sediments in the Desert West of Langshan. (Ph.D Thesis), Inner Mongolia Agricultural University, Hohhot, China, 2021 (in Chinese with English abstract).
[36] X. Wang, F. Wang, F. Du, B. Zhou, Y. Chang, W. Hu, The physical environment evolution and trajectories of drift sand in southeastern Alxa of China, Geogr. Res. (4) (2002) 479–486 (in Chinese with English abstract).
[37] F. Wang, D. Sun, F. Chen, J. Bloemendal, F. Guo, Z. Li, Y. Zhang, B. Li, X. Wang, Formation and evolution of the Badain Jaran Desert, North China, as revealed by a drill core from the desert centre and by geological survey, Palaeogeogr. Palaeoclimatol. Palaeoecol. 426 (2015) 139–158.
[38] H. Zhao, B. Li, X.F. Wang, T.J. Cohen, Y.X. Fan, H.Y. Yang, K.Q. Wang, Y.W. Sheng, S.A. Zhan, S.H. Li, T. Wang, X.L. Wang, F.H. Chen, Evolution and migration of the highest megadunes on Earth, Global Planet. Change 225 (2023), 104133.
[39] Z. Dong, G. Qian, L. Ping, G. Hu, Investigation of the sand sea with the tallest dunes on earth: China's Badain jaran sand sea, Earth Sci. Rev. 120 (120) (2013) 20–39.
[40] X. Yang, L. Scuderi, L. Tao, P. Paillou, H. Li, J. Dong, B. Zhu, W. Jiang, A. Jochems, G. Weissmann, Formation of the highest sand dunes on Earth, Geomorphology 135 (1–2) (2011) 108–116.
[41] Z. Li, Q. Chen, S. Dong, D. Zhang, X. Yu, C. Zhang, Applicability of rare earth elements in eolian sands from desert as proxies for provenance: a case study in the Badain Jaran Desert, Northwestern China, Catena 207 (2021), 105647.

[42] A. Liang, Z. Zhang, I. Lizaga, Z. Dong, Y. Zhang, X. Liu, F. Xiao, J. Gao, Which is the dominant source for the aeolian sand in the Badain Jaran Sand Sea, Northwest China: fluvial or gobi sediments? Catena 225 (2023), 107011.
[43] W.V. Boynton, Cosmochemistry of the Rare Earth Elements: Meteorite Studies, Developments in Geochemistry, Elsevier, 1984, pp. 63–114.
[44] M. Ferrat, D.J. Weiss, S. Strekopytov, S. Dong, H. Chen, J. Najorka, Y. Sun, S. Gupta, R. Tada, R. Sinha, Improved provenance tracing of Asian dust sources using rare earth elements and selected trace elements for palaeomonsoon studies on the eastern Tibetan Plateau, Geochem. Cosmochim. Acta 75 (21) (2011) 6374–6399.
[45] G. Chen, Z. Dong, C. Li, W. Shi, T. Shao, W. Nan, J. Yang, Provenance of aeolian sediments in the Ordos deserts and its implication for weathering, sedimentary processes, Front. Earth Sci. 9 (2021) 544.
[46] D.R. Muhs, The geochemistry of loess: Asian and North American deposits compared, J. Asian Earth Sci. 155 (2018) 81–115.
[47] J. Budahn, R. Schmitt, Petrogenetic modeling of Hawaiian tholeiitic basalts: a geochemical approach, Geochem. Cosmochim. Acta 49 (1) (1985) 67–87.
[48] J. Sun, Source regions and formation of the loess sediments on the high mountain regions of northwestern China, Quat. Res. 58 (3) (2002) 341–351.
[49] J. Sun, Provenance of loess material and formation of loess deposits on the Chinese Loess Plateau, Earth Planet Sci. Lett. 203 (3–4) (2002) 845–859.
[50] G. Wu, B. Xu, C. Zhang, S. Gao, T. Yao, Geochemistry of dust aerosol over the eastern pamirs, Geochem. Cosmochim. Acta 73 (4) (2009) 977–989.
[51] C. Zdanowicz, G. Hall, J. Vaive, Y. Amelin, J. Percival, I. Girard, P. Biscaye, A. Bory, Asian dustfall in the st. Elias mountains, yukon, Canada, Geochem. Cosmochim. Acta 70 (14) (2006) 3493–3507.
[52] B.-m. Jahn, S. Gallet, J. Han, Geochemistry of the Xining, Xifeng and Jixian sections, Loess Plateau of China: eolian dust provenance and paleosol evolution during the last 140 ka, Chem. Geol. 178 (1–4) (2001) 71–94.
[53] Z. Ding, J. Sun, S. Yang, T. Liu, Geochemistry of the Pliocene red clay formation in the Chinese Loess Plateau and implications for its origin, source provenance and paleoclimate change, Geochem. Cosmochim. Acta 65 (6) (2001) 901–913.
[54] S.R. Taylor, S.M. McLennan, The Continental Crust: its Composition and Evolution, 1985.
[55] X.-M. Liu, D.S. Hardisty, T.W. Lyons, P.K. Swart, Evaluating the fidelity of the cerium paleoredox tracer during variable carbonate diagenesis on the Great Bahamas Bank, Geochem. Cosmochim. Acta 248 (2019) 25–42.
[56] E.H. De Carlo, W.J. Green, Rare earth elements in the water column of lake vanda, McMurdo dry valleys, Antarctica, Geochem. Cosmochim. Acta 66 (8) (2002) 1323–1333.
[57] J.J. Braun, M. Pagel, J.P. Muller, P. Bilong, A. Michard, B. Guillet, Cerium anomalies in lateritic profiles, Geochem. Cosmochim. Acta 54 (3) (1990) 781–795.
[58] Y. Yang, X. Fang, A. Galy, E. Appel, M. Li, Quaternary paleolake nutrient evolution and climatic change in the western Qaidam Basin deduced from phosphorus geochemistry record of deep drilling core SG-1, Quat. Int. 313 (2013) 156–167.